水中ウォータージェット流れのシミュレーションに適する改良CIP-CUP法とその検証

An Improved CIP-CUP Method for Submerged Water Jet Flow Simulation

彭　國義, 富山県立大・工, 富山県小杉町黒河 5180, E-mail: peng@pu-toyama.ac.jp
石塚　勝, 富山県立大・工, 富山県小杉町黒河 5180, E-mail: ishizuka@pu-toyama.ac.jp
葉山眞治, 富山県立大・工, 富山県小杉町黒河 5180, E-mail: hayama@pu-toyama.ac.jp
Guoyi PENG, Toyama Prefectural Univ., 5180 Kurokawa, Kosugi, Toyama 939-0398, JAPAN
Masaru ISHIZUKA, Toyama Prefectural Univ., 5180 Kurokawa, Kosugi, Toyama 939-0398, JAPAN
Shinji HAYAMA, Toyama Prefectural Univ., 5180 Kurokawa, Kosugi, Toyama 939-0398, JAPAN

The original CIP-CUP method has been improved by introducing the state equation of Tait form so as to present the real pressure-density relation of complex water. Computational results of 1D shock tube problem and 2D shear driven cavity water flow have demonstrated its accuracy and validity of compressible and incompressible flow simulations. The method has been applied to the flow simulation of impulsively started submerged water jet. The computational result agrees with the experimental one of Gharib et al. The result shows that vortex rings are formed at the head of jet and move forward as developing of the jet flow. The total circulation of vortices increases linearly with the vortex formation time during the jet injection.

1. INTRODUCTION

The present research is concerned on the topic relevant to the direct numerical simulation of the submerged water. Although many experimental studies have been made from fundamental and practical viewpoints [1][2], there are a few theoretical and numerical ones [3]. In the flow of the submerged water jets, the compressibility of the fluid becomes prominent near the jet periphery because of cavitation inception, while in the far field the flow is essentially incompressible. Both the compressible and incompressible features coexist in the flow at the same time. It is difficult to construct suitable models to deal with both compressible and incompressible flows of the submerged water jet simultaneously. Simulations of the compressible flow and the incompressible flow are usually made by different numerical schemes. For the compressible flow, some elaborate schemes, such as the TVD scheme [4], have been developed but they are ineffective for the incompressible flow. On the other hand, schemes for the incompressible flow, such as the Marker and Cell (MAC) method [5], cannot treat phenomena associated with sharp discontinuities such as the submerged water jet flow.

A cubic interpolated pseudo-particle combined unified procedure (CIP-CUP) has been proposed [6], and then applied to various problems of fluid flow [7]. It has an advantage of treating both compressible and incompressible flows simultaneously. The unique feature that of this method is expected to be useful for the simulation of complex phenomena such as a submerged water jet where cavitation inception occurs in vortices around the jet periphery and cavitating regions reveal strong compressibility due to the growth and collapse of numerous bubbles.

The original CIP-CUP method is based on the CIP method proposed for solving hyperbolic equation governing the compressible flow. For the computation of incompressible liquid flow, an artificial compressibility is introduced according to the sound speed in the fluid under assumption of adiabatic fluid. Although the treatment makes it possible to calculate the incompressible flow, the process cannot present the physical property of the fluid correctly. On this consideration, the CIP-CUP procedure is improved by introducing a state equation of Tait form, which presents the pressure-density relation of water. Had been validated through computations of benchmark problem, the improved CIP-CUP method (henceforth denoted as CCUP-I) is applied to the simulation of two-dimensional submerged water jet flow. In this way, the water is treated as a real compressible fluid with small compressibility. But cavitation is not included for the main purpose of the present work is to seek a possibility to the simulation of complex submerged water jet flow.

2. GOVERNING EQUATIONS

The flow to be researched is assumed to be two-dimensional. Then, conservation equations of mass and momentum are respectively given by

$$\frac{\partial \rho}{\partial t} + u_i \frac{\partial \rho}{\partial x_i} = -\rho \frac{\partial u_i}{\partial x_i}, \tag{1}$$

$$\frac{\partial u_i}{\partial t} + u_j \frac{\partial u_i}{\partial x_j} = -\frac{\partial p}{\rho \partial x_i} + \frac{\partial \tau_{ij}}{\rho \partial x_j}, \tag{2}$$

where

$$\tau_{ij} = \mu\left(\frac{\partial u_i}{\partial x_j} + \frac{\partial u_j}{\partial x_i}\right) - \delta_{ij}\frac{2}{3}\mu\frac{\partial u_k}{\partial x_k} \qquad (i, j, k = 1, 2),$$

in which x_1 and x_2 are respectively the two components of a position vector, u_1 and u_2 the two components of a velocity vector, ρ the fluid density, p the fluid pressure, t the time, μ the dynamic viscosity coefficient which is assumed to be constant, δ_{ij} the Kronecker delta function ($\delta_{ij} = 1$ if $i = j$ and $\delta_{ij} = 0$ if $i \neq j$).

Concerning the conservation equation of energy, the water temperature is assumed to be constant. Therefore it can be removed from a set of governing equations. Instead, for making Eqs.(1) and (2) close, we introduce the state equation of water in general form of $p = p(\rho, T)$, from which we obtain,

$$\frac{dp}{dt} = \frac{\partial p}{\partial \rho}\frac{d\rho}{dt} + \frac{\partial p}{\partial T}\frac{dT}{dt}. \tag{3}$$

For a constant temperature, it is simplified as,

$$\frac{dp}{dt} = \frac{\partial p}{\partial \rho}\frac{d\rho}{dt}. \tag{4}$$

This is the case of barotropic fluids and a pressure-density relation can be given by Tait equation [8] as follows,

$$\frac{p+B}{p_0+B} = \left(\frac{\rho}{\rho_0}\right)^{\gamma}, \tag{5}$$

where B and γ are respectively constant values, 3.049×10^8 Pa and 7.15 for bubbly water [9], and the subscript 0 denotes a reference

state which will be taken to be the atmospheric one here. For B=0, Eq.(5) reduces to the adiabatic case for gas media. From Eqs.(1), (4) and (5), we obtain the following governing equation of pressure,

$$\frac{\partial p}{\partial t}+u_i\frac{\partial p}{\partial x_i}=-\gamma\left(p+B\right)\frac{\partial u_i}{\partial x_i}\ . \tag{6}$$

Equations (1), (2) and (6) are a set of governing equations, which should be solved.

3. NUMERICAL PROCEDURE

The governing equations in the preceding section can be written in the following form,

$$\frac{\partial f}{\partial t}+u_i\frac{\partial f}{\partial x_i}=g\ \ , \tag{7}$$

where

$$f=\{\rho,u_i,p\}^T$$

$$g=\left\{-\rho\frac{\partial u_i}{\partial x_i},\left(-\frac{\partial p}{\rho\partial x_i}+\frac{\partial\tau_{ij}}{\rho\partial x_j}\right),-\gamma(p+B)\frac{\partial u_i}{\partial x_i}\right\}^T,\ \ (i,\ j=1,2)\ ,$$

in which the bracket {} denotes a matrix and T the transposition of the matrix. Following the CIP-CUP procedure, the equations are respectively split into a non-advection phase and an advection phase as follows,

$$\frac{\partial f}{\partial t}=g\ , \tag{8}$$

$$\frac{\partial f}{\partial t}+u_i\frac{\partial f}{\partial x_i}=0\qquad (i=1,\ 2) \tag{9}$$

The equation (8) of non-advection phase is further decomposed into inviscid and viscous parts, which are computed by a finite difference method. A tentative value of inviscid pressure p^{**} at the new time step of $t+\Delta t$ is computed from by the following Poisson equation,

$$\frac{1}{\rho^n}\frac{\partial^2 p^{**}}{\partial x_i\partial x_i}-\frac{1}{\rho^{n2}}\frac{\partial\rho^n}{\partial x_i}\frac{\partial p^{**}}{\partial x_i}-\frac{p^{**}-p^n}{\gamma(p^n+B)\Delta t^2}=\frac{1}{\Delta t}\frac{\partial u_i^n}{\partial x_i}\ , \tag{10}$$

where the superscript n denotes the value of the previous time step t, Δt the time interval. The new density ρ^* and the inviscid velocity u_i^{**} are calculated according to the inviscid pressure p^{**}. Then non-advection phases of velocity u_i^* and the pressure p^* are obtained by adding the viscosity term to the inviscid part. Their final values are expressed as follows.

$$\rho^*=\rho^n+\frac{\rho^n}{\gamma(p^n+B)}(p^{**}-p^n)\ , \tag{11}$$

$$u_i^*=u_i^n+\Delta t\left(-\frac{1}{\rho^n}\frac{\partial p^{**}}{\partial x_i}+\frac{\partial\tau_{ij}}{\rho^n\partial x_j}+Q_u\right), \tag{12}$$

$$p^*=p^{**}+\Delta t\left(-\gamma\left(p^n+B\right)\frac{\partial^2\tau_{ij}}{\rho^n\partial x_i\partial x_j}\Delta t+Q_p\right), \tag{13}$$

where the superscript ** denotes the value of inviscid part and * the value of non-advection phasw. Q_u and Q_p are artificial viscosity terms, which are necessary to reduce numerical oscillations of solutions [10]. These terms are given as follows [11],

$$Q_u=-\frac{1}{\rho}\frac{\partial q_v}{\partial x_i},\qquad Q_p=-(\gamma-1)q_v\frac{\partial u_i}{\partial x_i} \tag{14}$$

The artificial viscosity is given by,

$$q_v=-\alpha\rho\left(\Delta U_i\sqrt{\gamma(p+B)/\rho}+0.5(\gamma+1)\left(\Delta U_i\right)^2\right), \tag{15}$$

where

$$\Delta U_i=min\left\{0,\Delta u_i=\left(\frac{\partial u}{\partial x}\Delta x\right)_i\right\}\qquad (i=1,2)\ ,$$

in which α is a control parameter for the artificial viscosity and it is usually set around 0.5-1.0 for the case of gas flow [11], and a smaller value for liquid flow.

The above non-advection phase is numerically calculated by the finite difference based on the MAC algorithm, and a fully staggered arrangement of velocity components and pressure has been adopted [12]. The velocity components are taken at the centers of cell surfaces in the same directions of velocity components, while the pressure and density are taken at the cell center. This staggered arrangement has an advantage to suppress oscillations in the pressure due to a strong coupling between velocity and pressure. The first-order spatial derivatives of flow variables, those are required in the computations of advection phase, are defined at the same positions as dependent flow variables. The Poisson equation of pressure is solved by the under relaxation technique for the high speed of pressure propagation in liquid flow.

The equation (9) of advection phase is solved by the cubic interpolated pseudo-particle (CIP) method. The value of advection phase $f(\boldsymbol{x},t+\Delta t)$ at the time step $t+\Delta t$ is obtained by shifting an interpolated profile of non-advection phase as follows,

$$f(\boldsymbol{x},t+\Delta t)=F(\boldsymbol{x}-\boldsymbol{u}\Delta t,t)+f_v^*\ , \tag{16}$$

where the function $F(\boldsymbol{x}-\boldsymbol{u}\Delta t,t)$ is a cubic spline defined by the results of the non-advection phase and first-order spatial derivatives [13]. f_v^* is a numerical viscosity term to improve the accuracy of CIP computation in the local of sharp discontinuity and it is given as [14],

$$f_v^*=\beta\Delta t^2\frac{\partial^2 f^*}{\partial x_i\partial x_i}\ , \tag{17}$$

in which β is a control parameter of constant greater than zero for the numerical viscosity. The first-order spatial derivatives are given as follows from equation (7).

$$\frac{\partial}{\partial t}\left(\frac{\partial f}{\partial x_i}\right)+u_j\frac{\partial}{\partial x_j}\left(\frac{\partial f}{\partial x_i}\right)=\frac{\partial g}{\partial x_i}-\frac{\partial u_j}{\partial x_i}\frac{\partial f}{\partial x_j}\quad ,\quad (i=1,\ 2) \tag{18}$$

The same as primary field variables, the first-order derivatives are independently preserved and calculated by advection of CIP method. This is different from other conventional methods, where the first-order spatial derivatives are usually estimated by using the preserved value of primary variables. It enables one to construct an interpolation function with relatively less computation grids. The cubic spline function for interpolation, which is essential to the calculation of advection phase, is defined between adjacent positions of the arrangement for the flow variable.

Summarizing above, the whole procedure of CCUP-I method can be expressed as follows,

$$f^{n+1}=\boldsymbol{L_2}\boldsymbol{L_1}f^n\ . \tag{19}$$

where $\boldsymbol{L_1}$ denotes the operator of non-advection phase and $\boldsymbol{L_2}$ the operator of advection phase. f^{n+1} is the computation result of flow variables at the time step of $t+\Delta t$.

4. NUMERICAL RESULTS

4.1 Validity of compressible flow simulation

For compressible flow, the CCUP-I method is the same as the CIP-CUP method, which has good accuracy for the computation of advection phase. For the purpose of validation, we have used the CCUP-I method to the flow simulation of one-dimensional

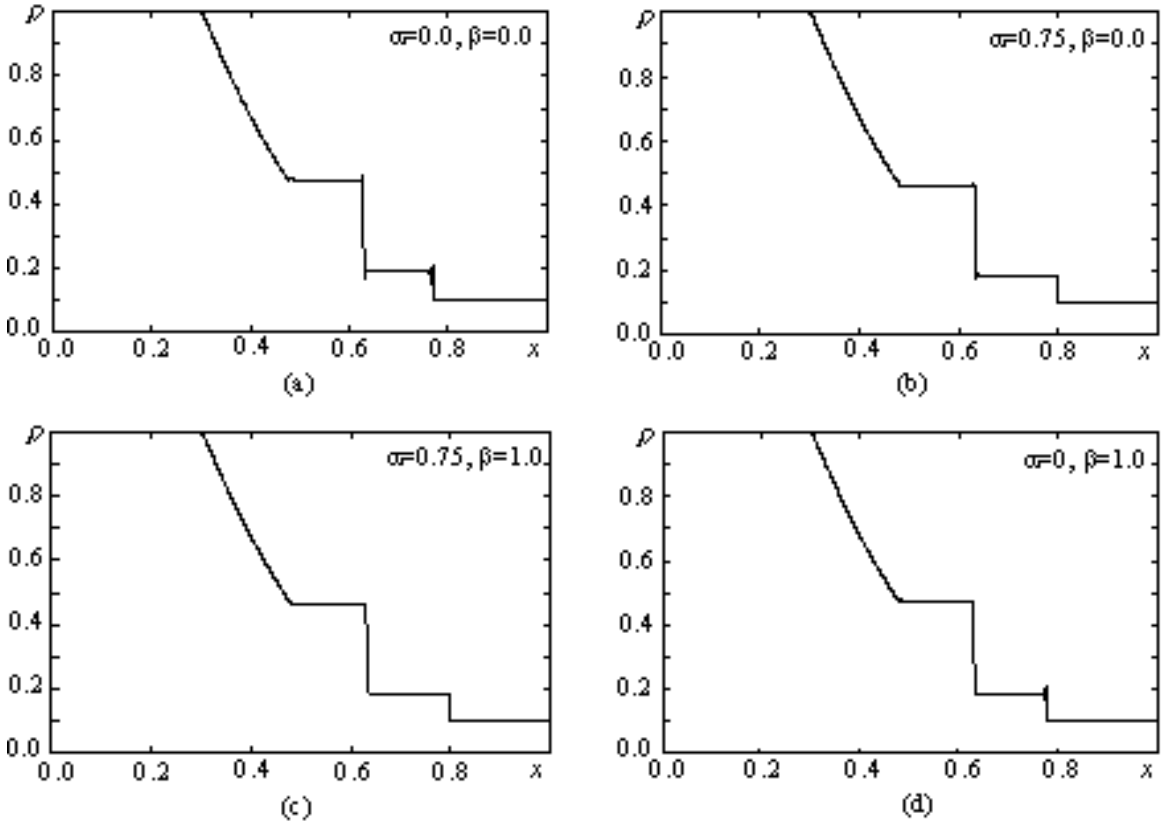

Fig.1 Computational result of density distribution

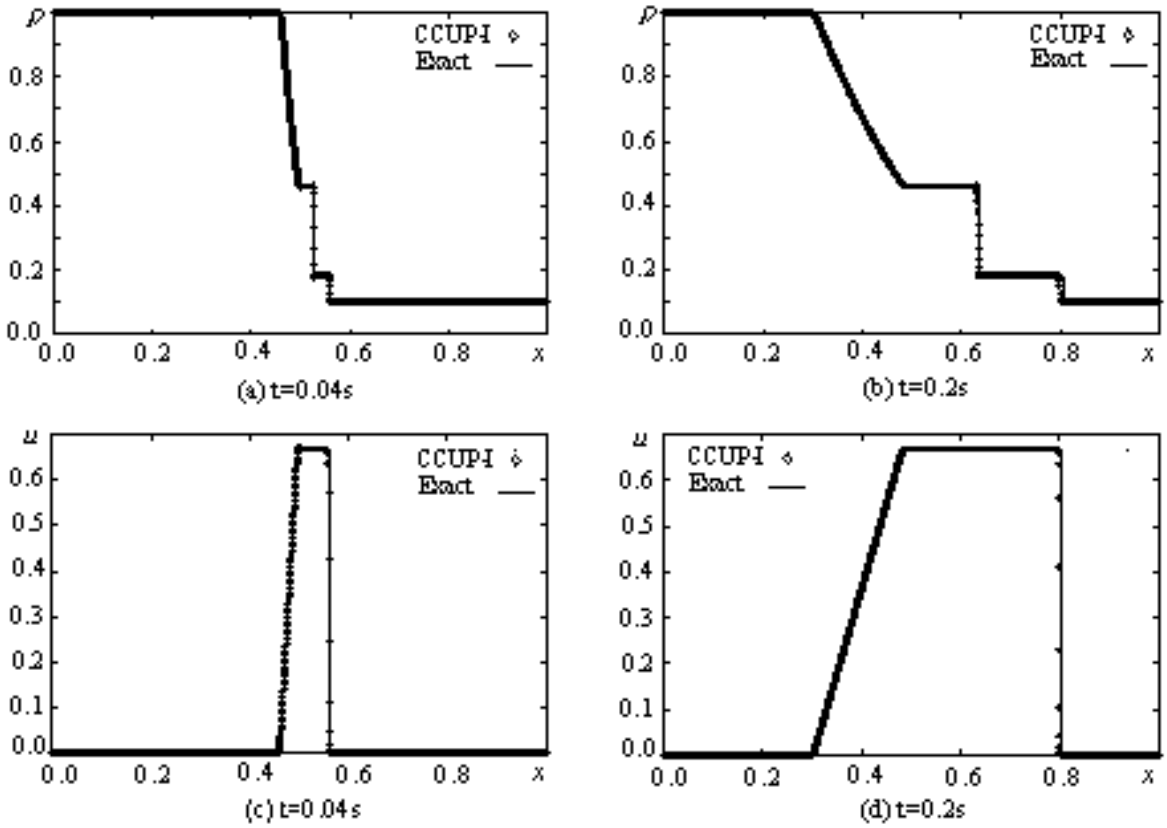

Fig.2 Comparison of numerical results to exact solutions

shock tube problem where the initial condition is given as,

p=1.0, ρ=1.0 for $0 \le x \le 0.5$, and p=0.1, ρ=0.1 for $0.5 < x \le 1.0$.

The specific heat ratio is γ=5/3. Figure 1 shows the effects of artificial viscosity coefficient α for non-advection computation and the numerical viscosity β for advection computation. From the figure we understand that α and β should employ a value

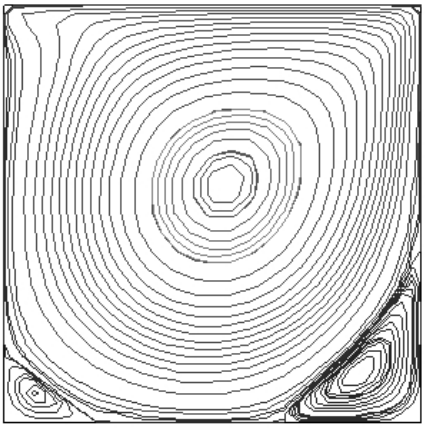

(a) Contours of stream function

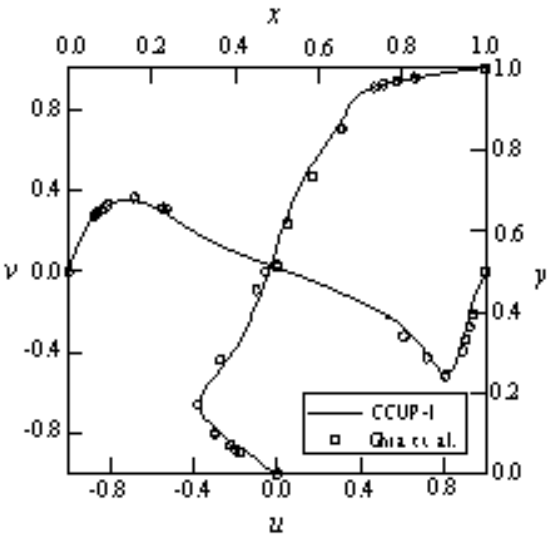

(b) Velocity profiles

Fig.3 Shear-driven cavity water flow (*R*e=1000)

greater than zero in order to suppress the numerical jump shown in Fig.1 (b) and the numerical oscillation shown in Fig.1 (d). Figure 2 (a) and (b) show numerical results of density distribution at the instant *t*=0.04s and t=0.2s while (c) and (d) do the velocity distribution the same instant. Analytic exact solutions are shown with solid line. The computational result coincides with the analytic one well.

4.2 Validity of incompressible flow simulation

As for the simulation of incompressible flow, a critical point is how to handle the conservation equation of mass. The CCUP-I method deals with the liquid as a real compressible fluid with very small compressibility by introducing the state equation representing the pressure-density relation. For the purpose of validation, a simulation of two-dimensional shear driven cavity water flow, which is a popular benchmark problem of incompressible flow, has been treated. Figure 3 (a) shows the result of the streamline distribution at the instant of t=30s when the flow is thought to be well developed. The corresponding velocity profiles along centric lines are shown in Fig.3 (b). The computational result is in good agreement with that given by Ghia et al. [15]. The present procedure is found to be valid.

4.3 Application to submerged water jet flow simulation

4.3.1 Boundary and initial conditions

The schematic configuration of submerged water jet to be

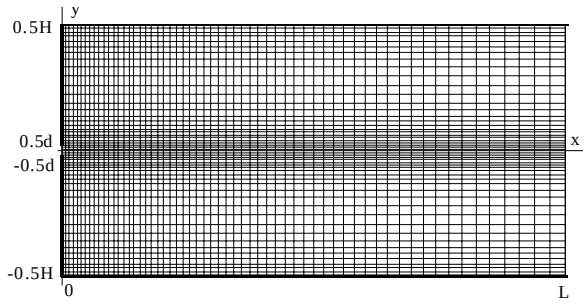

Fig.4 Configuration of submerged water jet

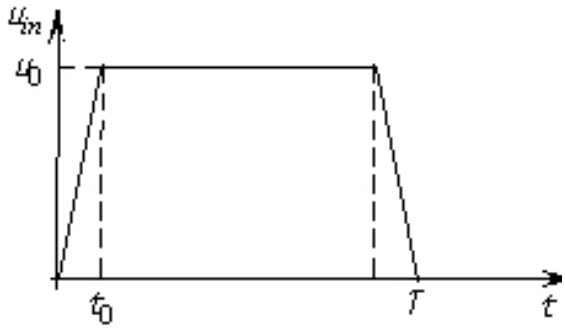

Fig.5 Profile of jet injection velocity versus time

considered here is shown in Fig.4, in which the jet is injected into still water from an orifice at a given velocity. The computation domain is composed of a rectangular plane of width *H*=0.5m and length L=1.0m. The orifice is set in the coaxial form with the horizontal centric line and its diameter is *d*=0.02m. The boundary conditions for velocity are set as follows:

u=u_{in} and v=0 $u = u_{in}$ and $v = 0$ for $-0.5d < y < 0.5d$ at $x = 0$,

u=v=0 for $-0.5H \le y \le -0.5d$, $0.5d \le y \le 0.5H$, (x = 0),

$u = v = 0$ for $0 < x < L$ at $y = \pm 0.5H$,

For the pressure, Neumann boundary conditions of pressure gradient given by Eq.(7) are imposed at the inlet and all solid wall boundaries.

Near the outlet boundary of $-0.5H \le y \le 0.5H$ at $x = L$, the flow remains unsteady for the value of time consideration. The presence of vortices propagating downstream makes it difficult to specify an accurate pressure condition. Various treatments to determine flow quantities on the boundary are reported [16]. The following one giving the best result is applied here.

$$\begin{cases} \dfrac{\partial v}{\partial x} = 0, \quad \dfrac{\partial u}{\partial x} = -\dfrac{\partial v}{\partial y} \\ \dfrac{\partial p}{\partial y} = -\rho\left(\dfrac{\partial v}{\partial t} + v\dfrac{\partial v}{\partial y}\right) + \left(\dfrac{\partial \tau_{xy}}{\partial x} + \dfrac{\partial \tau_{yy}}{\partial y}\right) \end{cases} \tag{20}$$

The pressures on the outlet boundary is obtained by integration of $\partial p/\partial y$ performed along the boundary by imposing $p = p_0$ at the first point of x=L and y=0.

As the special request of CIP method, boundary conditions for the first spatial derivatives of flow variables are also need to be defined. In the present computation, the normal gradient is given by the second-order one-side finite difference and the tangential gradient is given by the second-order central finite difference.

As shown in Fig.5, the jet is impulsively started with the following time dependent inlet velocity corresponding to Gharib et al.'s experiments [17],

$$u_{in} = \begin{cases} u_0 t/t_0 & (0 \le t < t_0) \\ u_0 & (t_0 \le t \le T - t_0) \\ u_0 (T - t)/t_0 & (T - t_0 < t \le T) \end{cases} \tag{21}$$

where t_0 is an acceleration time, T the duration time of jet injection and u_0 a constant velocity.

Computational meshes (60×50) are shown in Fig.4. The step of time marching is taken to be $\Delta t = 1.0\times10^{-5}$ s. The mesh size and the interval of time step are adjusted by performing mesh and time step refinement so as to obtain accurate solutions in the region of interest. For the Poisson equation, a convergence criterion ε of relative changes of solutions is given to be 1.0×10^{-3}.

4.3.2 Vortex formation and total circulation

The flow of submerged water jet is unsteady. Vortex rings are formed around the jet as time lapse. The total circulation of vortex rings can be calculated by

$$\Gamma_{total} = \iint_{\Omega} \omega \, d\Omega \ , \tag{22}$$

where $\boldsymbol{\omega}$ denotes the vorticity of vortices formed in the flow and $\boldsymbol{\Omega}$ the computation domain. According to the experiment of Gharib *et al.* [17], the total circulation is a function of vortex formation time defined as,

$$t^* = \bar{u}_{in} t / d \ , \tag{23}$$

where $\bar{u}_{in} = t^{-1}\int_0^t u_{in} dt$ is an average velocity during jet injection. Figure 6 shows computational results of the one impulse jet injection corresponding to Gharib et al's experiment, where the acceleration time of jet injection is t_0=0.001s and the duration time of jet injection is T=0.6s. The velocity u_0 is taken to be 0.2m/s here to avoid cavitation. Taking u_0 as the reference velocity and the orifice diameter d as the reference length, we get the Reynolds number $R_e = 3.984\times10^3$.

Figure 6 (a), (b) and (c) are respectively distributions of vorticity contour at the instants when t^* equals 5, 10 and 40. They agree with the experimental ones. Figure 7 shows the variation of the total circulation, where the total circulation Γ_{total} is normalized as,

$$\Gamma^* = \Gamma_{total} / \bar{u}_{in} d \ . \tag{24}$$

The computational results are in good agreement with the experimental ones shown by circles except in initial stages of vortex formation. The discrepancy of the initial stages may be due to that the motion vortices is influenced by the inlet solid boundary. It is difficult to distinguish the real vortices with their bound vortices from the boundary. Therefore, the computational domain of the total circulation is shifted a little from the boundary here to avoid the circulation of the wall bound vortices. So, the total circulation is to be less than the experimental one in the initial stages. As vortices move away from the boundary, the effect of boundary becomes smaller and the computational result approaches the experimental one.

Figure 7 shows some computational results with different mesh size. The results do not scatter so much, and they are not so sensitive to the mesh size within the range of adopted meshes. The figure demonstrates that the total circulation of vortices

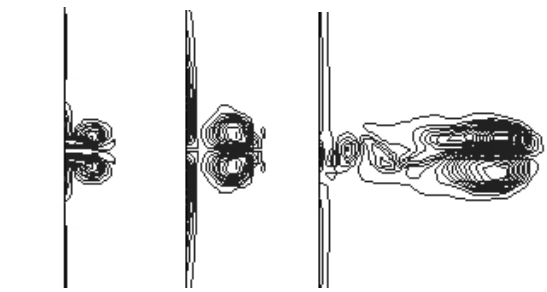

(a) t^*=5 (b) t^*=10 (c) t^*=40

Fig.6 Vortexes formed in submerged water jet (T=0.6s)

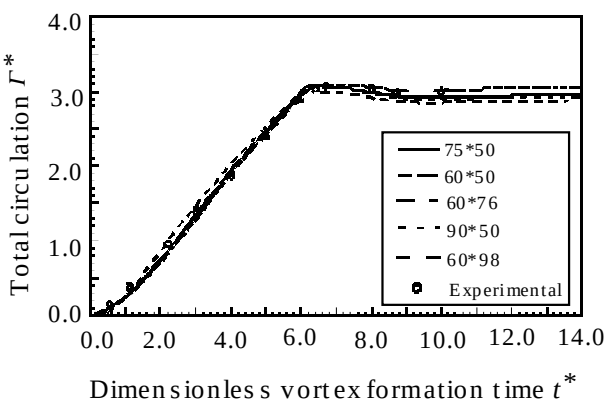

Fig.7 Total circulation evaluated for impulse jet (T=0.6s)

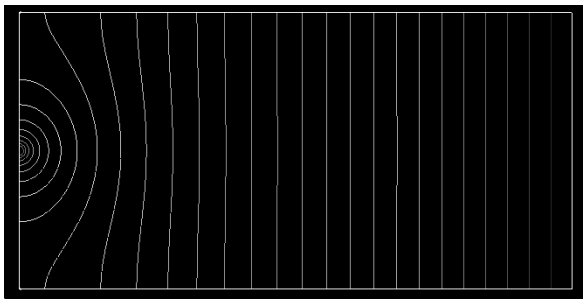

(a) At t^*=0.1

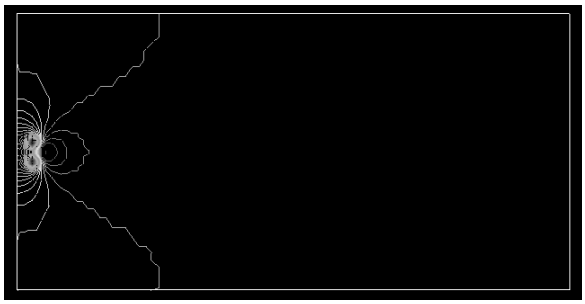

(b) At t^*=5

Fig.8 Pressure distributions of impuse jet

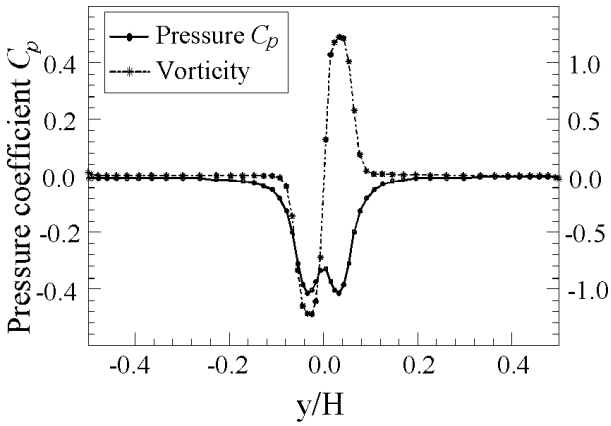

Fig. 9 Pressure and vorticity distributions on section crossing vortex centers (t^*=5)

linearly increases with the vortex formation time within the duration of jet injection. The circulation maintains a constant value for a while and then decays according to the time lapse after the jet injection stopped.

4.3.3 Pressure distribution

Corresponding to the flow structure shown above, the pressure distribution is an important dynamic index having great effect on the performance of submerged water jet. Figure 8 shows pressure distributions in the different time stages. At the instant of t^*=0.1, the isobar distribution of Fig.8 (a) demonstrates that the pressure wave radiates at the initial of the jet injection. The pressure wave decays within a short time. At the instant of t^*=5, the pressure distribution is shown in Fig.8 (b) where low-pressure regions are formed. Compared with the Fig.6 (a), the figure shows that local areas of vortex ring appear to be low-pressure regions. The pressure distribution in vortices is shown in Fig.9 with solid line, where the abscissa is the vertical section through the vortex centers, and the ordinate is the pressure indicated by the following pressure coefficient,

$$C_p = \frac{p - p_0}{0.5\rho u_0^2}. \tag{25}$$

The dash line shows corresponding vorticity distribution, which is concentrated at the vortex centers located on the jet periphery. The pressure reaches its minimum values at the vortex centers. As the vortex radii increases, the pressure rises sharply.

It is well known that the cavitation inception occurs when a nucleus (e.g. microscopic bubble or particle with air trapped in it crevices) is explored to a sufficiently low pressure to cause unstable growth and collapse of cavity. Rigorous cavitation inception criteria have been discussed in [18]. The conditions for cavitation inception are typically indicated by the cavitation inception index,

$$\sigma_i = \frac{p_i - p_v}{0.5\rho u_0^2} \tag{26}$$

where p_i is the static pressure, and p_v the vapor pressure of the liquid. The cavitation inception index takes its minimum value at the centers of vortexes. Thus, cavitation inceptions easily take place at the centers of vortexes on the periphery of the jet. This agrees with an experimental finding that the lowest pressure occurred in the core of primary vortexes, where cavitation inception occurred [19]. Cavitation experiments show that the cavitation inception index is closely connected to the jet flow structure [20][21]. The reason may be due to that the local static pressure determining the cavitation inception index is mainly dependent on the vortex structure, the size and the strength of the vortex.

5. CONCLUDING REMARKS

The original CIP-CUP method has been improved by introducing the state equation of Tait form so as to present the pressure-density relation of water correctly. The method is capable of calculating incompressible and compressible flow simultaneously and thought to be advantageous to the direct simulation of complex water flow. Its numerical property has been investigated through computations of compressible 1D shock tube problem. Computational results of 2D shear driven cavity water flow have proved its validation of incompressible flow simulation.

The improved CIP-CUP method has been applied to the flow simulation of impulsively started submerged water jet. Computation has confirmed the experimental results of Gharib et al. The result shows that vortex rings are formed at the head of jet and move forward as developing of the jet flow. Their vorticity concentrates at the vortex centers located around the jet periphery. The total circulation of vortices increases linearly with the vortex formation time within the duration of jet injection.

Local areas of vortex centers appear to be low-pressure regions. The pressure of vortices reaches its minimum value at vortex centers and increases sharply with increasing of vortex radii. Thus the cavitation inception index takes the minimum value at vortex centers located around the jet periphery where cavitation inceptions easily take place.

REFERENCES

[1] Ymamaguti, A and Shimizu, S., Erosion due to Impingement of Cavitation Jet, Trans. ASME, Journal of Fluid Engineering, vol.109, (1987), 442-447.

[2] Ooi, K. K., Scale Effects on Cavitation Inception in Submerged Water Jets: A New Look, Journal Fluid Mechanics, Vol.151, (1985), 367-390.

[3] Lichtarowucz, A., Jet Cutting Technology, Kluwer Acdemic Publishers, 1992, 633.

[4] Harten, A., High Resolution Schemes for Hyperbolic Conservation Laws, Journal Computational Physics, Vol.49, (1983), 357-393.

[5] Haelow, F. H. and Welch, J, E., The Marker and Cell Method, Physics Fluids, Vol.8, (1965), 2182-2189.

[6] Yabe, T and Wang, P. Y., Unified Numerical Procedure for Compressible and incompressible fluid, Journal of the Physical Society of Japan, Vol.60, No.7, (1991), 2105~2108.

[7] Xiao, F. and Yabe, T., Computation of complex flow containing rheological bodies, Computation Fluid Dynamics Journal, Vol.8, No.1, (1999), 43-49.

[8] Prospertti, A. and Lezzi, A., Bubble dynamics in a compressible liquid. Part 1. First order theory, Journal Fluid Mechanics, Vol.168, (1986), 457-578.

[9] Fujikawa S. and Akamatsu T., Effects of the non-equilibrium condensation of vapor on the pressure wave produced by the collapse of a bubble in a liquid, Journal Fluid Mechanics, Vol.97, (1980), 481-512.

[10] Yabe, T., A Universal Cubic Interpolation Solver for Compressible and Incompressible Fluids, Shock Waves, Vol.1, (1991), 187-195.

[11] Utsumi, T., Differential algebraic hydrodynamics solver with cubic-polynomial interpolation, Computational Fluid Dynamics Journal, Vol.4, No.2, (1995), 225-238.

[12] Ferziger, J. H. and Milovan, P., Computational Methods for Fluid Dynamics, Springer, 2nd ed., (1999), 198-203.

[13] Yabe, T. and Aoki, T., A Universal Solver for Hyperbolic Equations by Cubic-Polynomial Interpolation, Computer Physics Communications, Vol.66, (1991), 219-242.

[14] Tang, H., Zhang, D. and Lee, C., Analysis and modification of CIP method for hyperbolic Equations, Computational Fluid Dynamics Jurnal, Vol.6, No.3, (1997), 227-236.

[15] Ghia, U., Ghia K. N. and Shin C. T., High-Re Solution for Incompressible Flow Using the Navier-Stockes Equations and a Multigrid Method, Journal Computational Physics, Vol.48, (1982), 387-411.

[16] Peyret, R. and Taylor, T. D., Computational Methods for Fluid Flow, Springer, 3ed., (1990), 78-79.

[17] Gharib, M., Rambod, E. and Shariff, K., Universal Time Scale for Vortex Ring Formation, Journal Fluid Mechanics, Vol.360, (1998), 121-140.

[18] Joseph, D. D., Cavitation and the State of Stress in a Flowing Liquid, Journal Fluid Mechanics, Vol.366, (1998), 367-378.

[19] O'Hern, T. J., An Experimental Investigation of Turbulent Shear Flow Cavitation, Journal Fluid Mechanics, Vol.215, (1990), 365-391.

[20] Gopalan, G., Katz, J. and Knio, O., The Flow Structure in the Near Field of Jets and Its Effect on Cavitation Inception, Journal Fluid Mechanics, Vol.398, (1999), 1-43.

[21] Katz, J. and O'Hern, T. J., Cavitation in Large Scale Shear Flow, Trans ASME Journal Fluids Engineering, Vol.108, (1986), 373-376.